Femtosecond Photoelectron Imaging on Pyridine: Ultrafast Electronic Dephasing from the $S_1(n\pi^*)$ State and Rydberg State Energetics

Masaaki Tsubouchi†

The Graduate University for Advanced Studies, Myodaiji, Okazaki 444-8585, Japan

Toshinori Suzuki*

Chemical Dynamics Laboratory, RIKEN, Wako 351-0198, Japan

Received: August 7, 2003; In Final Form: September 17, 2003

Ultrafast electronic dephasing from the $S_1(n\pi^*)$ state and the energetics of the $n = 3$ Rydberg states of pyridine were studied by time-resolved photoelectron imaging in conjunction with (1+2′) resonance-enhanced multiphoton ionization (REMPI) via the S_1 state. The lifetime at the S_1 origin was determined to be 32 ± 5 ps from the decay of the total photoionization signal. Photoelectron energy and angular distributions observed for (1+2′) REMPI clearly indicated that two-photon ionization from the S_1 state is being enhanced by the resonance with singlet $3s(n^{-1})$ and $3p(n^{-1})$ Rydberg states that have not been clearly observed before. The electronic energies of the $3p_x(\delta=0.57)$ and $3p_y(\delta=0.50)$ Rydberg states were determined for the first time, to be 56 120 and 57 140 cm^{-1}, respectively.

I. Introduction

Femtosecond time-resolved photoelectron imaging (TRPEI) combined with resonance-enhanced multiphoton ionization (REMPI) is a novel experimental means to probe excited-state dynamics of molecules.[1−3] In our previous work, we have demonstrated this methodology in examining the intersystem crossing (ISC) in pyrazine (1,4-diazabenzene).[1−6] The TRPEI allowed observation of ionization from the S_1 and the triplet states as a function of pump−probe time delay, thereby visualizing both the S_1 decay and the triplet growth in real time. For ionization, the $(1+1')$[2,3] and (1+2′) REMPI[1,4−6] schemes were employed, and both provided consistent results. In the (1+2′) case, ionization was enhanced by the resonance with the $3s(n^{-1})$ and $3p(n^{-1})$ Rydberg states. Because the TRPEI allowed highly accurate measurements of the photoelectron angular distributions (PADs), these PADs were utilized to explore rotational wave packet motions,[5] ionization dynamics,[3,5,6] and the properties of low-lying Rydberg states.[6] A similar experiment has also been preformed on pyridazine (1,2-diazabenzene) more recently.[7]

In the present study, we explore ultrafast dynamics of pyridine (azabenzene) by femtosecond (1+2′) TRPEI (Figure 1). Pyridine is the most fundamental azabenzene molecule that possesses nonbonding (n) and π electrons. The photophysics and photochemistry of pyridine have been subject to numerous theoretical and experimental investigations: Innes et al. have given a comprehensive review on the studies reported before 1988.[8] Pyridine had been believed to be a totally nonfluorescent molecule until 1977 when Yamazaki and Baba discovered weak fluorescence in the gas phase.[9] The fluorescence quantum yield has been determined to be $\Phi_F = 5.9 \times 10^{-5}$ at the S_1 0^0 level.[10,11] Such a low fluorescence quantum yield is due to both ISC and internal conversion (IC) processes, as the measured

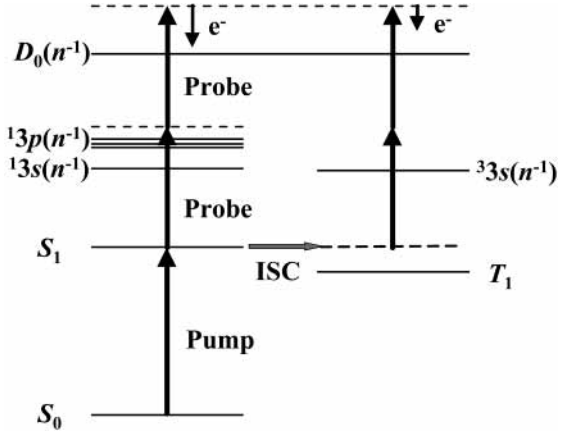

Figure 1. (1+2′) REMPI of pyridine.

ISC quantum yield is 0.3.[11] The direct observation of the S_1 decay rate was performed by Yamazaki and co-workers for a number of S_1 levels of pyridine vapor in 1982, and its lifetime was 42 ps at the S_1 0^0 level.[12] More recently, Zhong et al. have performed time-resolved mass spectrometry in the molecular beam.[13] The lifetime of S_1 in solution is in the range of 9−23 ps, depending on the solvent.[14] Although the deactivation from the $S_2(\pi\pi^*)$ state may involve isomerization to the Dewar form,[14,15] the ISC and IC are the only important processes from the S_1 state. The triplet state of pyridine is clearly distorted, as observed by electron spin−echo experiments by Schmidt and co-workers.[16] Recent ab initio and density functional calculations have confirmed the boat-shaped T_1 state with mixed $(\pi\pi^*)$ and $(n\pi^*)$ character.[17] Cai and Reimers have reported extensive computational studies on the low-lying valence states of pyridine.[18]

In our previous works, (1+2′) REMPI of pyrazine and pyridazine were enhanced by the resonance with 3s and 3p Rydberg states.[6,7] Therefore, the REMPI scheme may be more correctly expressed as a (1+1′+1′) process. A similar resonance

* Corresponding author. E-mail: toshisuzuki@riken.jp.
† Present address: Chemical Dynamics Laboratory, RIKEN.

10.1021/jp036333a CCC: $25.00
Published on Web 11/22/2003

effect is anticipated also for pyridine studied in the present work. Femtosecond photoelectron imaging with the (1+1′+1′) scheme provides an interesting and novel opportunity to explore low-lying molecular Rydberg states. One-photon electronic transitions to these states are usually obscured by much stronger absorption to the valence states, and multiphoton ionization via these Rydberg states are not highly efficient for their very short lifetimes. For instance, the lifetime of the 3s state of pyridine has been estimated to be 700 fs.[19] In the present study, Rydberg states are accessed by (1+1′) excitation from the ground state, which is much more efficient than nonresonant two-photon excitation to the Rydberg states, and ionization via these short-lived Rydberg states is induced by a femtosecond probe laser pulse.

The (1+1′) excitation to the Rydberg states via S_1 restricts the observable Rydberg states to be the (n^{-1}) Rydberg states, which is another advantage of TRPEI for Rydberg spectroscopy. Azabenzene molecules have close lying cationic states with different electron holes in the n and π orbitals, which gives rise to two different Rydberg series with the (n^{-1}) and (π^{-1}) ion cores. Pyridine is well-known for its extremely close (n^{-1}) and (π^{-1}) cationic states that are separated by slightly more than 1000 cm^{-1}, which suggests that all the Rydberg states with different ion cores and the same principal and orbital quantum numbers are separated by only 1000 cm^{-1}. In the past, the characters of lowest ionic states were subject to extensive investigations.[20] Utsunomiya et al. observed the photoelectron kinetic energy dependence of the anisotropy parameter in the ultraviolet photoelectron spectroscopy (UPS) of pyridine and compared it with that of 2,6-dimethylpyridine, for which the energetic ordering of the cationic states were already known.[21] Piancastelli et al. performed UPS of pyridine using synchrotron radiation.[22] Reineck et al. have compared the UPS of pyridine and pyridine-d_5,[23] whereas Brundle, Robin, and Kuebler examined the perfluoro effect on the UPS of pyridine.[24] All these reached the conclusion that the lowest cationic state is n^{-1}. Berg et al. have analyzed the polarization dependence of the (2+1) REMPI of pyridine via the lowest 3s Rydberg state, which also suggested that the lowest cationic state is n^{-1}.[25] Recent ab initio molecular orbital calculations confirmed these conclusions.[26] When two-color excitation is employed via the S_1 state, observation of the Rydberg states is limited to the series converging to the n^{-1} cationic state, because the configuration mixing between the $S_1(n\pi^*)$ and the other ($\pi\pi^*$) state is small. Therefore, the Rydberg states observed by our TRPEI via the S_1 state will be unambiguously the n^{-1} Rydberg states.

With the selection of ion core and observation of photoelectron energy and angular distributions, assignments are provided for the low-lying (n^{-1}) Rydberg states of pyridine.

II. Experimental Section

The experimental setup and the data collection procedure employed in the present study are identical to those in our previous TRPEI study.[5,6] Very briefly, a 4% pyridine sample gas was prepared by passing the N_2 carrier gas over the liquid sample at a room temperature and was continuously expanded into the vacuum at a stagnation pressure of 500 Torr through a pinhole 50 μm in diameter. The supersonic jet thus produced was sampled by a skimmer 0.8 mm in diameter, and the resulting beam was introduced into an ionization chamber, where the background pressure (beam on) was ca. 10^{-7} Torr. The rotational temperature of pyridine in the beam was determined to be 10−20 K from a rotational analysis of the S_1 0_0^0 band in the (1+1) REMPI spectrum measured with a nanosecond laser system.

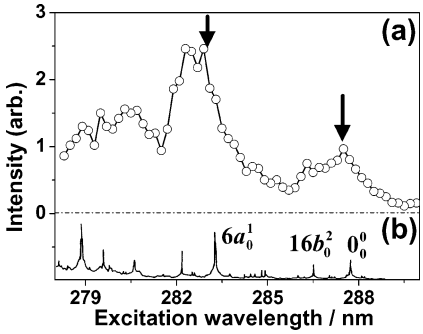

Figure 2. (a) REMPI (upper) spectrum in the molecular beam and (b) absorption (lower) spectrum in the bulk at a room temperature of the $S_1 \leftarrow S_0$ transition of pyridine. The former was obtained by femtosecond two-color (1+2′) REMPI with a tunable UV pump and 401 nm probe light. The time delay between the pump and the probe lasers was kept at 2 ps. The latter is the spectrum obtained with a nanosecond laser by Sushida et al.[11] Arrows show the excitation wavelengths used in this work.

The Nd:YLF-pumped Ti:Sapphire laser generated a 1 kHz pulse train of 802 nm femtosecond light, and each pulse was split into two equal intensity beams by a dichroic mirror. One beam pumped a commercial optical parametric amplifier (OPA) to generate the tunable UV *pump* light at 275−295 nm. The other beam was used to generate a *probe* light either at 401 nm by second harmonic generation in a thin BBO I crystal or at 350−370 nm by exciting another OPA. The pump (~1 μJ) and the delayed probe (~5 μJ) pulses intersected the molecular beam. The cross-correlation width of the pump and probe laser beams was measured to be ~150 fs.

The molecules in the beam were ionized by (1+2′) REMPI. The generated photoelectrons were accelerated parallel to the molecular beam in a velocity mapping[27] electric field and were detected by a position sensitive imaging detector that consisted of a 40 mm diameter dual microchannel plate backed by a P20 phosphor screen. The field-free region of the electron flight path (450 mm) was shielded against stray magnetic fields by a μ-metal tube. Light emission from the screen was coupled out of the vacuum chamber by a fiber bundle and was recorded by an intensified video-rate charge-coupled-device (CCD) camera with 768 × 572 pixels. Observed images were inverse-Abel transformed for obtaining 3D photoelectron scattering distributions. To measure the total photoelectron signal, the current passing through the phosphor screen was monitored.

III. Results

A. Temporal Profiles of the Total Photoelectron Current. Figure 2 shows the $S_1(^1B_1) \leftarrow S_0(^1A_1)$ excitation spectrum of pyridine measured by femtosecond two-color (1+2′) REMPI with 401 nm probe light. The time delay between the pump and the probe pulses was maintained to be 2 ps. For comparison, the absorption spectrum of pyridine vapor at a room temperature measured with a nanosecond laser by Sushida et al. is also shown in the figure.[11] In the present work, 0_0^0 and $6a_0^1$ bands located at 34 771 and 35 313 cm^{-1}, respectively,[8] were used for photoexcitation. Due to the limited spectral resolution obtainable with the femtosecond laser, these two bands are not clearly separated from their adjacent $16b_0^2$ (at 34 909 cm^{-1}) and $16b_0^2 6a_0^1$ (at 35 451 cm^{-1}) sidebands,[28] respectively.

The total photoelectron signal measured at the pump wavelengths of 287.5 nm (0_0^0; $S_1 \leftarrow S_0$) and 283 nm ($6a_0^1$; $S_1 \leftarrow S_0$) are presented as a function of the pump−probe time delay in Figure 3a,b, respectively. In both cases, the signal intensity

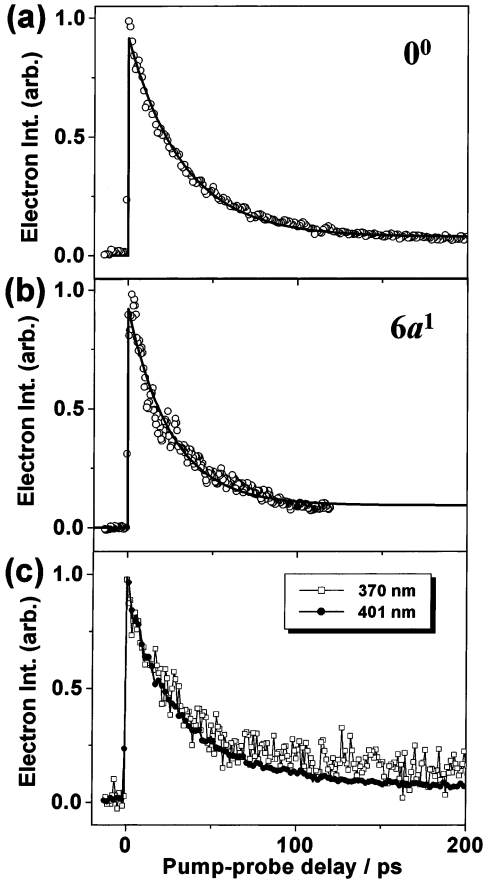

Figure 3. Temporal profiles of the total photoelectron currents measured with the pump wavelengths of (a) 287.5 nm (0_0^0; $S_1 \leftarrow S_0$) and (b) 283 nm ($6a_0^1$; $S_1 \leftarrow S_0$). The probe wavelength was 401 nm in both cases. Open circles and solid lines show the observed data points and best-fit exponential decay functions. (c) Probe wavelength dependence of the temporal profiles observed for the pump wavelength of 287.5 nm (0_0^0; $S_1 \leftarrow S_0$) with 370 nm (open squares) and 401 nm (solid circles) probe light.

TABLE 1: Decay Time Constant τ, the Ratio A_2/A_1, and the Quantum Yield of Intersystem Crossing Φ_{ISC} of the $S_1(n\pi^*)$ State of Pyridine

vib state	E_{vib}/cm^{-1} [a]	A_2/A_1	τ/ps (this work)	τ/ps	Φ_{ISC}[b]
0^0	0	10.8	32(5)	42(2)[b]	0.30
$16b^2$	138			60(2)[b]	0.28
$6a^1$	542	8.9	25(5)	42(2)[b]	0.30
$16b^26a^1$	670			54(2)[b]	0.27
$6a^2$	1084			38(2)[b], 32(1)[c], 15[d]	0.20

[a] Vibrational energy in the S_1 state.[8] [b] Picosecond fluorescence decay.[12] [c] Picosecond photoelectron spectroscopy.[29] [d] Femtosecond mass spectroscopy.[13] The pump wavelength 277 nm employed is 2 nm shorter than the excitation wavelength of $6a_0^2$ band.

rapidly diminished exponentially, yet to some nonzero residual values. After 100 ps, there is virtually no further change of the photoelectron signal intensity in Figure 3a. The time profiles were analyzed by the least-squares fitting to the functional form of $I(t) = A_1 + A_2 \exp(-t/\tau)$, where t is the pump−probe time delay. The lifetime τ and the ratio A_2/A_1 thus determined are summarized in Table 1 along with the literature values.[12,13,29] The lifetimes were 32 and 25 ± 5 ps at the 0^0 and $6a^1$ vibronic states, respectively, which are in fair agreement with the previously reported values. Yamazaki et al. reported the excitation wavelength dependence of the fluorescence lifetime for the S_1 state of pyridine.[12,30] As the excitation wavelength changed from 288 to 274 nm, the lifetime decreased gradually

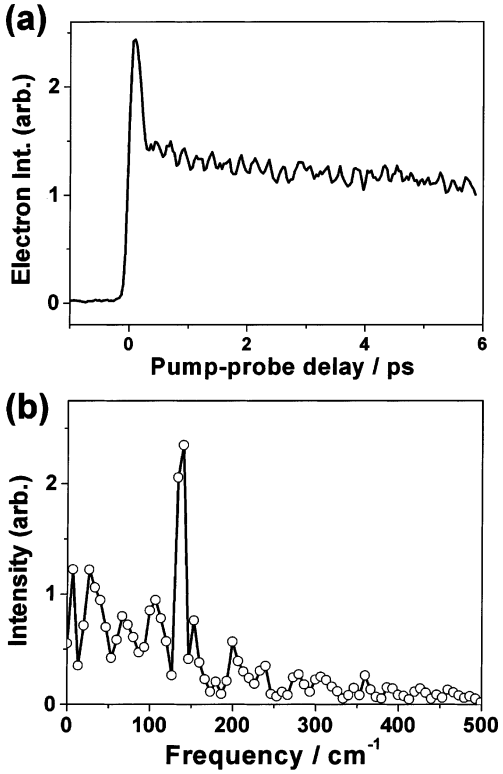

Figure 4. (a) Temporal profile of the total photoelectron current measured with the 287.5 nm pump and the 401 nm probe wavelengths. The periodic oscillation at a 200−300 fs interval is seen in the profile. (b) Amplitude spectrum obtained by the Fourier transformation of the oscillatory component of the temporal profile.

except for the combination bands associated with the nontotally symmetric vibrations of 10a and 16b.[30]

Figure 3c presents the probe wavelength dependence of the total photoelectron signal observed with 287.5 nm pump light. At the 370 nm probe wavelength, the nonzero component appearing at a long delay time became larger than that probed by using 401 nm light. This difference is due to probe wavelength dependence of the triplet state ionization efficiency.

The temporal profile of the photoelectron current observed using the 287.5 nm pump and the 401 nm probe light at short-time range is expanded in Figure 4a. The sharp spike at zero time delay and the periodic oscillation with the 200−300 fs interval are seen in the profile. Because the sharp spike has the same width with the cross-correlation time between the pump and probe pulses, it is ascribed to a coherent nonlinear response of a molecule that is not discussed in detail here. The Fourier transform of the oscillatory component is shown in Figure 4b. The peak energy of ∼140 cm^{-1} agrees with that of the $16b^2$ vibration (138 cm^{-1}).[28] Therefore, the periodic oscillation observed in the temporal profile is due to the vibrational quantum beat created by coherent excitation of the 0_0^0 and the $16b_0^2$ bands. This result accords with our excitation spectrum where the 0_0^0 and the $16b_0^2$ bands are not resolved. No other beat frequency was discernible in the Fourier transform with our signal-to-noise ratio, which is in agreement with the feature of the absorption spectrum. Because the total photoionization current almost exclusively reflects the time-evolution of the singlet character, as discussed below, and no vibrational dephasing (IVR) occurs near the origin, the observed beat is not damped as a function of time.

B. Time-Resolved Photoelectron Energy and Angular Distributions. Time-resolved photoelectron images measured

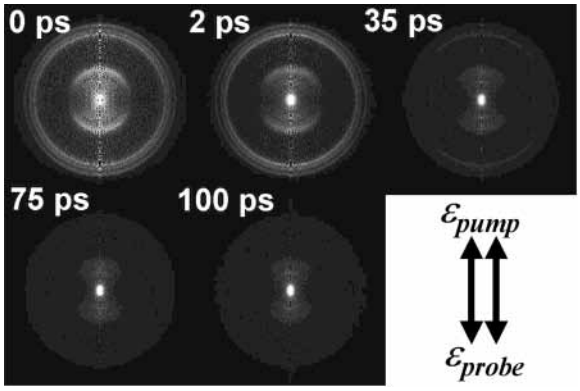

Figure 5. Time-resolved photoelectron images of pyridine taken at pump−probe delay times of 0, 2, 35, 75, and 100 ps. Pump and probe wavelengths are 287.5 and 401 nm, respectively. Polarization of the pump and probe laser beams are parallel to each other and in the vertical direction in the figure, as indicated by arrows.

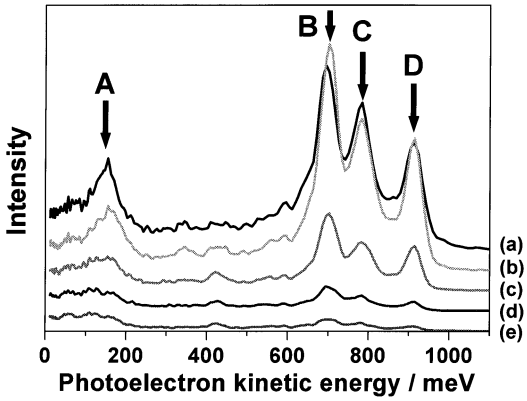

Figure 6. Time-resolved photoelectron kinetic energy distributions obtained with the 287.5 nm pump and the 401 nm probe wavelengths at the pump−probe delay times of (a) 0, (b) 2, (c) 35, (d) 75, and (e) 100 ps. Highest possible photoelectron kinetic energy corresponding to ionization to the zero vibrational level in the cation is ca. 1.23 eV. The arrows with A−D indicate the four components considered in the analysis.

with the 287.5 nm pump and the 401 nm probe light at the delay times of 0, 2, 35, 75, and 100 ps are shown in Figure 5. These images are the slices through the 3D photoelectron scattering distributions obtained by an inverse Abel transformation of the original images. The polarization vectors of the pump and probe laser beams are parallel to each other and in the vertical direction in the figure. Three sharp outer rings and the diffuse inner ring are clearly seen. The inner ring exhibits strong anisotropy, whereas outer rings are rather isotropic. The intensities of all rings diminish for longer pump−probe delay times. This suggests that these rings are due to ionization from S_1. However, close examination reveals that a low-energy component is persistent at longer time delays.

Figure 6 presents the time-resolved photoelectron kinetic energy distributions (PEDs) extracted from the images shown in Figure 5. Note that the low energy photoelectrons consist of two components; a diffuse band around ∼100 meV, and a sharper peak A centered at 151 meV. The peak width of the components A−D were obtained to be 59, 73, 57, and 52 meV in fwhm, respectively, when these were fitted to the Lorentzian profiles. Similar fitting with Gaussian profiles provided the fwhm of 64, 71, 44, and 60 meV, respectively. The widths of the B−D peaks are close to the resolution of our apparatus, $\delta E \sim 50$ meV at 1 eV. The intensity of the peak A diminishes at longer delay times similarly with the three sharp peaks (B−D) at the higher energies. The photoelectron signal less than 150 meV seems to remain even at long time delays. Because the detectable state at 100 ps is only the triplet state populated by ISC, it is highly likely that the diffuse band corresponds to photoelectrons generated by ionization from the T_1 state. The sharp peaks in PEDs indicate that these ionization processes occur with the vibrational propensity rule $\Delta v = 0$ via intermediate Rydberg states.[6] However, in the case of pyrazine, the ionization component from T_1 was also sharp, and its intensity increased clearly. The ionization intensity from the triplet state is much weaker for pyridine.

The energies of the zero vibrational levels, T, of the intermediate Rydberg states are obtained using the following formula, which is valid for the (1+1′+1′) REMPI scheme via the Rydberg states,[6]

$$\mathrm{PKE} = T(\mathrm{Rydberg}) + h\nu_2 - \mathrm{IP} \qquad (1)$$

where PKE is the photoelectron kinetic energy, IP is the adiabatic ionization potential, and ν_2 is the probe laser frequency. The energies of Rydberg states calculated with the IP of 74 740 cm^{-1},[8] are listed in Table 2. The quantum defect was found to be quite large ($\delta = 0.85$) for the state ($T = 51\,020$ cm^{-1}) associated with the peak A, which suggests that this state is the singlet 3s Rydberg state. On the other hand, the values of $\delta = 0.5-0.6$ indicate that the three states at $T = 55\ 390$, 56 120, and 57 140 cm^{-1} are the singlet 3p Rydberg states. From the analogy with the energy gap between the singlet 3s and the triplet 3s states (S-T gap) in pyrazine of only 500 cm^{-1},[6] the photoelectron signal appearing at the lower energy side of the peak A is assignable to ionization from the triplet state via the triplet 3s Rydberg state.

Figure 7 shows the time dependence of the photoelectron intensities of each peak obtained by the least-squares fitting of the time-resolved PEDs to five Lorentzian profiles. The alphabet A−D corresponds to each component in the PEDs shown in Figure 6. At short delay times within 5 ps, the intensities of C and D exhibit rapid change due to the anisotropy decay. Notice that the phases of modulation differ for ionization via these Rydberg states. At 43 ps, signatures of the half revivals of the rotational wave packet are anticipated but not seen clearly, presumably due to the limited signal-to-noise ratio. Interestingly, the A and B signals did not exhibit strong modulations.

TABLE 2: Observed Rydberg States of Pyridine

	state	PKE/meV	T/cm^{-1}	δ	β_2[a]	MRDCI[b]	VUV[b]	T obs[c]	(2+1) REMPI[d]
A	3s ($^1A_1$)	151	51 020	0.85	1.4	49 910	50 650	50 669	50 685
B	3p_z ($^1A_1$)	694	55 390	0.62	0.9	54 050	55 890	55 250[e]	
C	3p_x ($^1B_1$)	784	56 120	0.57	0.9	55 080			
D	3p_y ($^1B_2$)	910	57 140	0.50	1.1	57 040			

[a] Anisotropy parameters determined from the image at the pump−probe delay time of 2 ps. [b] Reference 26. [c] Reference 8. [d] Reference 19. [e] In ref 8, this state was assigned to 3p_x ($^1B_1$).

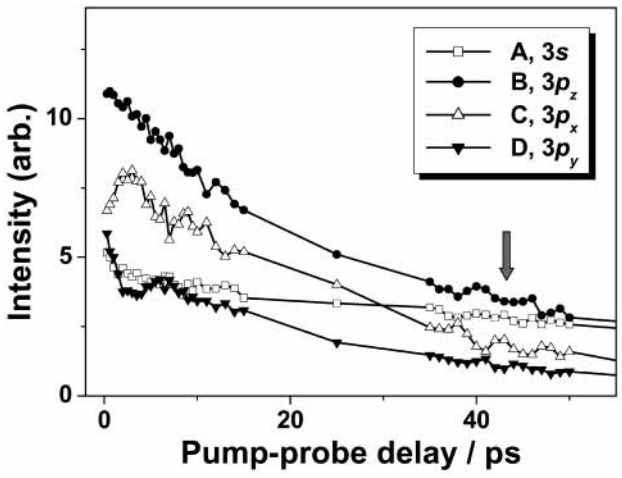

Figure 7. Temporal profiles of the energy selected photoelectron intensities. A−D indicate the components of the photoelectron kinetic energy distributions shown in Figure 6.

The PADs obtained by (1+2′) REMPI with parallel pump and probe polarization were analyzed by the least-squares fitting to the following function.[31]

$$I(t;\theta) \propto 1 + \beta_2(t)P_2(\cos\theta) + \beta_4(t)P_4(\cos\theta) + \beta_6(t)P_6(\cos\theta) \quad (2)$$

where $P_L(\cos\theta)$ denotes the Lth-order Legendre polynomial and θ is the polar angle between the laser polarization and the photoelectron **k** vector. The time evolutions of the anisotropy parameters, β_2, β_4, and β_6, determined for each photoelectron energy component are shown in Figure 8. The magnitude of β_6 was found to be negligible in all cases. Although the measured values are rather scattered, the rotational anisotropy decays in the first 2.5 ps are clearly seen in the time evolution of β_2 and β_4 obtained for the C and D components. In general, the PAD is expected to be more anisotropic in ionization from an s Rydberg state than from a p state.[32] The large anisotropy parameter ($\beta_2 = 1.4$) of peak A and the smaller parameters ($\beta_2 = 0.9 \sim 1.1$) of peaks B−D support our assignment of their electron orbital angular momentum. When the total ionization intensity (Figure 7) and β parameters (Figure 8) are compared, the phases of the anisotropy decay (either increasing or decreasing) do not necessarily agree with each other. This is because the modulation in the REMPI intensity is provided by the ratio of the parallel and perpendicular dipole moment magnitudes for the Rydberg ← S_1 transition, whereas the modulation in the β value originates from variation of the photoelectron outgoing partial waves with parallel and perpendicular transitions from the Rydberg state to the ionization continuum.

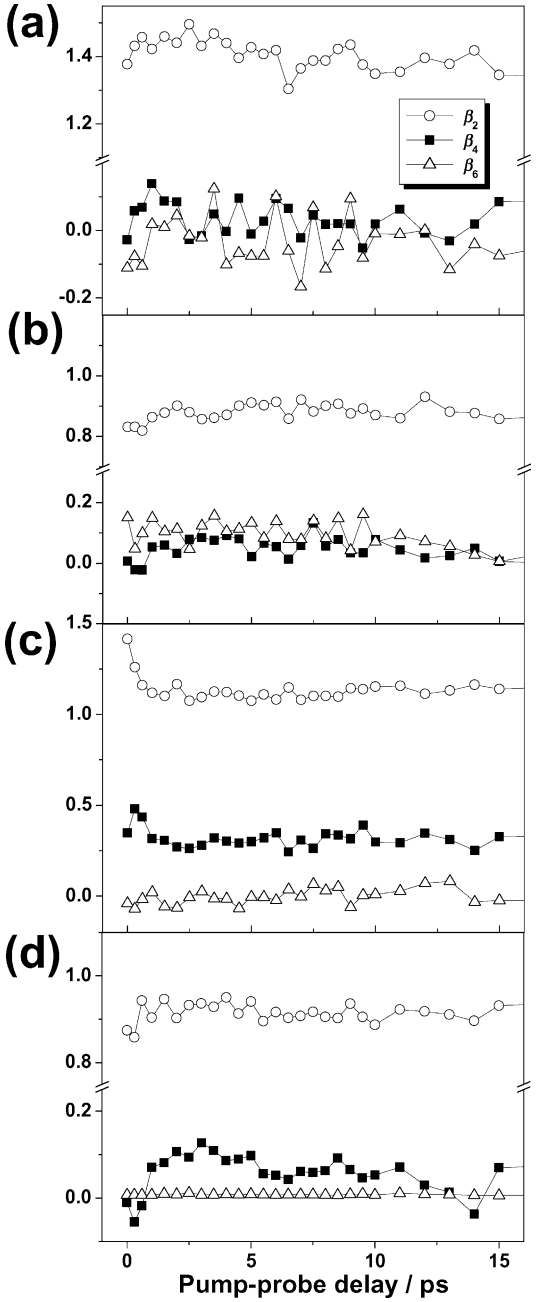

Figure 8. Time evolutions of the anisotropy parameters, β_2, β_4, and β_6, of the energy selected photoelectron angular distributions generated by ionization via the singlet (a) 3s, (b) 3p$_x$, (c) 3p$_y$, and (d) 3p$_z$ Rydberg states.

IV. Discussion

A. Electronic Dephasing of the S_1 State. From the S_1 0^0 state of pyridine, three deactivation processes are anticipated: $S_1 \rightarrow S_0$ fluorescence decay, $S_1 \rightarrow S_0$ internal conversion, and $S_1 \rightarrow T$ intersystem crossing. The very small fluorescence quantum yield ($\Phi_F = 5.9 \times 10^{-5}$)[12] implies that the first one is unimportant. Because the yield for ISC has been reported to be $\Phi_{ISC} = 0.3$,[12] the yield of IC is regarded as 0.7.

The temporal profiles of the total photoelectron signal are described as the sum of the decaying S_1 component and the growing triplet component, although the latter is quite small in this case. The molecules after undergoing IC to the S_0 state are hardly ionized, because the probe wavelength is too long for making any one-photon electronic transition to the resonance state from S_0.

In our previous studies, the dynamics of pyrazine[1,4,33] and pyridazine[7] have been investigated by TRPEI. In the case of pyrazine whose quantum yield of ISC from the $S_1(n\pi^*)$ state is known to be 1,[30] the $T_1(n\pi^*)$ state populated by ISC was detected in the temporal profiles of total photoelectrons and time-resolved photoelectron images. On the other hand, the ISC quantum yield of the pyridazine $S_1(n\pi^*)$ state is smaller than 0.05.[34] Correspondingly, no evidence of the triplet state formation was observed by TRPEI. However, the following consideration is also required for interpreting these results. The triplet state created by ISC may be probed by ionization via the triplet 3s and 3p states, where the Franck−Condon factors between the triplet state and the Rydberg states peak at rather high excess

TABLE 3: Spectroscopic Values of Pyridine, Pyrazine, and Pyridazine

			ΔE_{ST}		^{1}3s(n^{-1})		^{3}3s(n^{-1})	
	S_1[a]	IP[a]	S_1-T_1	3s(n^{-1})	T	PKE	T	PKE
pyridine	34 771	74 740	5119	420	51 020[c]	1220[c]	50 600[c]	800[c]
pyrazine	30 876	74 915[b]	4056	500	50 700[d]	800[d]	50 200[d]	400[d]
pyridazine	26 649	70 220	4162	(500)	45 800[e]	500[e]	(45 300)	(∼0)

The unit is cm^{-1}. ΔE_{ST} is the S−T energy gap, and PKE is a photoelectron kinetic energy obtained by (1+2′) REMPI with 401 nm probe via the S_1 0^0 state. The numbers in parentheses are the estimated values as described in the text. [a] Reference 8. [b] Reference 39. [c] This work. [d] Reference 6. [e] Reference 7.

energies in the Rydberg states. This is evidenced in our TRPEI of pyrazine using the (1+1′) REMPI scheme where the Franck−Condon factor peaks at more than 1 eV above the adiabatic ionization potential.[2] Because the Rydberg states have the same potentials with that of D_0 (the ground cationic state), the Franck−Condon factor between the triplet state and the Rydberg states of pyrazine should also peak at 1 eV above the origin of the Rydberg state. In accordance with this energetic consideration, (1+2′) ionization of the triplet state of pyrazine has occurred only via the 3s Rydberg state for which the vibrational excess energy on the Rydberg state in (1+2′) REMPI is 5500 cm^{-1}.[6] No ionization via the 3p Rydberg state has been identified. For pyridine, the Franck−Condon factor is expected to peak at a comparably high excess energy with that in pyrazine. Then, ionization from the triplet state will not occur via the 3p Rydberg state with the 401 nm probe laser light, for the lack of an excess energy. The ionization of the triplet state should be mediated by the 3s Rydberg state.

Table 3 summarizes the energies of the S_1 and the Rydberg states, the S−T energy gaps, and the photoelectron kinetic energies obtained by eq 1 in the (1+2′) REMPI with 401 nm probe light via the S_1 0^0 states, for pyridine, pyrazine, and pyridazine. For ISC from the S_1 0^0 state, the vibrational energies of the triplet state populated by ISC are quite similar to each other for these three molecules. The photoelectron kinetic energy generated by ionization from the triplet 3s(n^{-1}) Rydberg state of pyridazine is estimated to be almost zero when it is ionized by 401 nm probe light. In our previous experiment on this particular molecule of pyridazine, the probe light shorter than 401 nm was also employed; however, the one-color signal induced by the shorter probe light was too strong to perform extensive measurements. The experiment on pyridazine using the 401 nm probe light may not be conclusive in ruling out the possibility of ISC from S_1. A more ideal way to examine the pyridazine case is the (1+1′) REMPI scheme.

B. Energetics of Rydberg States. The singlet Rydberg states of pyridine were observed in VUV absorption,[26,35] electron energy loss,[26] and one-color (2+1) REMPI spectra.[19,36] The energies of neutral and cationic electronic states were also calculated by the MRD-CI[26] and the SAC-CI methods.[37] He(I) UPS clearly identified the two lowest cationic states (n^{-1} and π^{-1}) of pyridine close in energy.[38]

The p Rydberg state of molecules is split into the *x*, *y*, and *z* components. In pyridine, the definition of the axes is such that the *x* axis is perpendicular to the molecular plane and the *z* is along the axis passing through the nitrogen atom in the molecular plane. Three 3p Rydberg states observed in the present work are assigned as in Table 2, from the comparison with the calculated energies of $T(3p_z) < T(3p_x) < T(3p_y)$ by the MRD-CI method.[26] Although Innes et al. tentatively assigned the state at $T = 55\,250$ cm^{-1} observed by Bolovinos et al.[35] to the $3p_x$-($^1B_1$) Rydberg state in their review article,[8] the result of the MRD-CI calculation suggests that this state is the $3p_z$($^1A_1$) Rydberg state ($T = 55\,390$ cm^{-1} in our measurement). The $3p_x$-($^1B_1$) and $3p_y$($^1B_2$) Rydberg states had not been observed in previous one-photon spectroscopies,[8] because strong one-photon photoabsorption to the $^1B_2 + {}^1A_1(\pi\pi^*)$ state, corresponding to the 1 $^1E_{2u}$ state of benzene, hindered observation of the weak excitations to these Rydberg states. Because the $^1B_2 + {}^1A_1$-($\pi\pi^*$) state is not accessed in the present study, the 3p(n^{-1}) Rydberg states were clearly observed.

TABLE 4: Term Values (cm^{-1}) and Quantum Defects of the 3s and 3p Rydberg States of Pyridine, Pyrazine, and Pyridazine

	^{1}3s(n^{-1})		^{1}3p$_x$(n^{-1})		^{1}3p$_y$(n^{-1})		^{1}3p$_z$(n^{-1})	
	T	δ	T	δ	T	δ	T	δ
pyridine	51 020	0.85	56 120	0.57	57 140	0.50	55 390	0.62
pyrazine[a]	50 700	0.87			56 800	0.54	55 000	0.65
pyridazine[b]	45 800	0.88					50 650[c]	0.63

[a] Reference 6. [b] Reference 7. [c] Tentatively assigned to the $3p_z$ state.

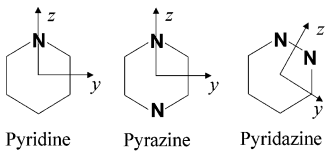

Figure 9. Definition of the molecular axes on pyridine, pyrazine, and pyridazine. The *x* axis is perpendicular to the molecular plane.

The energies of the singlet 3s and 3p Rydberg states of pyridine, pyrazine, and pyridazine determined by TRPEI are summarized in Table 4. Pyridine and pyridazine belong to the C_{2v} point group, and pyrazine belongs to the D_{2h} point group. The *x*-axis is perpendicular to the molecular plane for the three molecules. The *z*-axis is the C_2 symmetry axis for pyridine and pyridazine, and the N−N axis is for pyrazine (see Figure 9). The quantum defects of the 3s Rydberg states of these azabenzenes are very similar to each other ($\delta \sim 0.87$). In our previous study, for the 3p Rydberg state of pyridazine observed at $T = 50\,650$ cm^{-1} ($\delta = 0.63$), the projection quantum number to the molecular frame was not determined. However, comparing the quantum defects of the 3p Rydberg states of these azabenzenes, this particular state may be assigned to the $3p_z$ Rydberg state.

As seen in Figure 7, the partial ionization cross sections oscillate rapidly around $t = 0$. Because the $S_1(B_1) \leftarrow S_0(A_1)$ transition of pyridine corresponds to a parallel transition of an oblate top, the principal axis (the *x*-axis) of a molecule is aligned primarily along the polarization of pump light at the instant of photoexcitation.[33] Although the alignment rapidly diminishes due to the rotational dephasing, this provides some clues for the assignment of the Rydberg states. When the Rydberg $\leftarrow S_1$ transition in the ionization process is parallel or perpendicular, the excitation (ionization) efficiency is enhanced or reduced at the pump−probe delay time of 0 ps, respectively. From the time dependence shown in Figure 7, it is clear that peak D is a parallel transition and peak C is perpendicular. If we neglect the intensity borrowing transitions, these directions indicate the symmetry

of the Rydberg states to be $^1A_1$ $3p_z$ and $^1B_1$ $3p_x$ states. Notice that the one-photon transition of $3p_y \leftarrow S_1$ is symmetry forbidden and is clearly induced by either intensity borrowing or considerable distortion of the molecule. The fact that peaks A and B did not show clear time-dependent behavior also suggests that the transition dipole moments associated with these transitions are nearly isotropic, perhaps being affected by vibronic coupling effects.

V. Conclusion

Ultrafast electronic dephasing and energetics of Rydberg states of pyridine were studied by time-resolved photoelectron imaging in (1+2′) REMPI via the $S_1(n\pi^*)$ state. The lifetime of the S_1 0^0 state was determined to be 32 ± 5 ps from the decay of the total photoelectron current. Photoelectron energy and angular distributions clearly reveal the feature of ionization from the singlet $3s(n^{-1})$ and $3p(n^{-1})$ Rydberg states. The electronic energies of $3p_x(\delta=0.57)$ and $3p_y(\delta=0.50)$ Rydberg states were determined for the first time, to be 56 120 and 57 140 cm^{-1}, respectively.

Acknowledgment. This work was supported by a Grant-in-Aid from the Ministry of Education, Cluture, Sports, Science, and Technology of Japan under contract numbers 14204063 and 13127204 and also by Japan Science and Technology Corporation.

References and Notes

(1) Suzuki, T.; Wang, L.; Kohguchi, H. *J. Chem. Phys.* **1999**, *111*, 4859.
(2) Suzuki, T.; Whitaker, B. J. *Int. Rev. Phys. Chem.* **2001**, *20*, 313.
(3) Suzuki, T. Time-resolved photoelectron spectroscopy and imaging. In *Recent Advances in Chemical Reaction Dynamics*; Yang, X., Liu, K., Eds.; World Scientific: Singapore, 2003.
(4) Wang, L.; Kohguchi, H.; Suzuki, T. *Faraday Discuss.* **1999**, *113*, 37.
(5) Tsubouchi, M.; Whitaker, B. J.; Wang, L.; Kohguchi, H.; Suzuki, T. *Phys. Rev. Lett.* **2001**, *86*, 4500.
(6) Song, J. K.; Tsubouchi, M.; Suzuki, T. *J. Chem. Phys.* **2001**, *115*, 8810.
(7) Matsumoto, Y.; Kim, S. K.; Suzuki, T. *J. Chem. Phys.* **2003**, *119*, 300.
(8) Innes, K. K.; Ross, I. G.; Moomaw, W. R. *J. Mol. Spectrosc.* **1988**, *132*, 492.
(9) Yamazaki, I.; Baba, H. *J. Chem. Phys.* **1977**, *66*, 5826.
(10) Yamazaki, I.; Sushida, K.; Baba, H. *J. Chem. Phys.* **1979**, *71*, 381.
(11) Sushida, K.; Fujita, M.; Yamazaki, I.; Baba, H. *Bull. Chem. Soc. Jpn.* **1983**, *56*, 2228.
(12) Yamazaki, I.; Murao, T.; Yoshihara, K.; Fujita, M.; Sushida, K.; Baba, H. *Chem. Phys. Lett.* **1982**, *92*, 421.
(13) Zhong, D.; Diau, E. W.-G.; Bernhardt, T. M.; de Feyter, S.; Roberts, J. D.; Zewail, A. H. *Chem. Phys. Lett.* **1998**, *298*, 129.
(14) Chachisvillis, M.; Zewail, A. H. *J. Phys. Chem. A* **1999**, *103*, 7408.
(15) Wilzbach, K. E.; Raush, D. J. *J. Am. Chem. Soc.* **1970**, *92*, 2178; Chapman, O. L.; McIntosh, C. L.; Pacansky, J. *J. Am. Chem. Soc.* **1973**, *95*, 614. Ratajczak, E.; Sztuba, B. *J. Photochem.* **1980**, *13*, 233.
(16) Buma, W. J.; Groenen, E. J. J.; Schmidt, J. *Chem. Phys. Lett.* **1986**, *127*, 189. Buma, W. J.; Groenen, E. J. J.; Schmidt, J.; de Beer, R. *J. Chem. Phys.* **1989**, *91*, 6549.
(17) Buma, W. J.; Groenen, E. J. J.; van Hemert, M. C. *J. Am. Chem. Soc.* **1990**, *112*, 5447. Nagaoka, S.; Nagashima, U. *J. Phys. Chem.* **1990**, *94*, 4467.
(18) Cai, Z.-L.; Reimers, J. R. *J. Phys. Chem. A* **2000**, *104*, 8389.
(19) Dion, C. F.; Bernstein, E. R. *J. Chem. Phys.* **1995**, *103*, 4907.
(20) Al-Joboury, M. I.; Turner, D. W. *J. Chem. Soc.* **1964**, 4434.
(21) Utsunomiya, C.; Kobayashi, T.; Nagakura, S. *Bull. Chem. Soc. Jpn.* **1978**, *51*, 3482.
(22) Piancastelli, M. N.; Keller, P. R.; Taylor, J. W.; Grimm, F. A.; Carlson, T. A. *J. Am. Chem. Soc.* **1983**, *105*, 4235.
(23) Reineck, I.; Maripuu, R.; Veenhuizen, H.; Karlsson, L.; Siegbahn, K.; Powar, M. S.; Zu, W. N.; Rong, J. M.; Al-Shamma, S. H. *J. Electron Spectrosc. Relat. Phenom.* **1982**, *27*, 15.
(24) Brundle, C. R.; Robin, M. B.; Kuebler, N. A. *J. Am. Chem. Soc.* **1972**, *94*, 1466.
(25) Berg, J. O.; Parker, D. H.; El-Sayed, M. A. *Chem. Phys. Lett.* **1978**, *56*, 411.
(26) Walker, I. C.; Palmer, M. H.; Hopkirk, A. *Chem. Phys.* **1989**, *141*, 365.
(27) Eppink, A. T. J. B.; Parker, D. H. *Rev. Sci. Instrum.* **1997**, *68*, 3477.
(28) Jesson, J. P.; Kroto, H. W.; Ramsay, D. A. *J. Chem. Phys.* **1972**, *56*, 6257.
(29) Schultz, T.; Fischer, I. *J. Chem. Phys.* **1998**, *109*, 5812.
(30) Yamazaki, I.; Murao, T.; Yamanaka, T.; Yoshihara, K. *Faraday Discuss.* **1983**, *75*, 395.
(31) Yang, C. N. *Phys. Rev.* **1948**, *74*, 764.
(32) Cooper, J.; Zare, R. N. *J. Chem. Phys.* **1968**, *48*, 942.
(33) Tsubouchi, M.; Whitaker, B. J.; Suzuki, T. To be submitted.
(34) Holt, P. L.; Selco, J. I.; Weisman, R. B. *J. Chem. Phys.* **1986**, *84*, 1996.
(35) Bolovinos, A.; Tsekeris, P.; Philis, J.; Pantos, E.; Andritsopoulos, G. *J. Mol. Spectrosc.* **1984**, *103*, 240.
(36) Turner, R. E.; Vaida, V.; Molini, C. A.; Berg, J. O.; Parker, D. H. *Chem. Phys.* **1978**, *28*, 47.
(37) Kitao, O.; Nakatsuji, H. *J. Chem. Phys.* **1988**, *88*, 4913. Wan, J.; Hada, M.; Ehara, M.; Nakatsuji, H. *J. Chem. Phys.* **2001**, *114*, 5117.
(38) Baker, A. D.; Turner, D. W. *Philos. Trans. R. Soc. London A* **1970**, *268*, 131; Gleiter, R.; Heilbronner, E.; Hornung, V. *Helv. Chim. Acta* **1972**, *55*, 255; Kishimoto, N.; Ohno, K. *J. Phys. Chem. A* **2000**, *104*, 6940.
(39) Zhu, L.; Johnson, P. *J. Chem. Phys.* **1993**, *99*, 2322.